

# Repurposing 2D Diffusion Models with Gaussian Atlas for 3D Generation

Tiange Xiang<sup>1,2\*</sup>, Kai Li<sup>2†</sup>, Chengjiang Long<sup>2</sup>, Christian Häne<sup>2</sup>, Peihong Guo<sup>2</sup>,  
Scott Delp<sup>1</sup>, Ehsan Adeli<sup>1</sup>, Li Fei-Fei<sup>1†</sup>

<sup>1</sup>Stanford University, <sup>2</sup>Meta Reality Labs

<https://cs.stanford.edu/~xtiange/projects/gaussianatlas>

## Abstract

Recent advances in text-to-image diffusion models have been driven by the increasing availability of paired 2D data. However, the development of 3D diffusion models has been hindered by the scarcity of high-quality 3D data, resulting in less competitive performance compared to their 2D counterparts. To address this challenge, we propose repurposing pre-trained 2D diffusion models for 3D object generation. We introduce *Gaussian Atlas*, a novel representation that utilizes dense 2D grids, enabling the fine-tuning of 2D diffusion models to generate 3D Gaussians. Our approach demonstrates successful transfer learning from a pre-trained 2D diffusion model to a 2D manifold flattened from 3D structures. To support model training, we compile *GaussianVerse*, a large-scale dataset comprising 205K high-quality 3D Gaussian fittings of various 3D objects. Our experimental results show that text-to-image diffusion models can be effectively adapted for 3D content generation, bridging the gap between 2D and 3D modeling.

## 1. Introduction

Understanding the 3D world is crucial for numerous real-world applications. In this work, we focus on generative 3D modeling with the primary objective of generating high-quality 3D assets from given textural descriptions [13, 33].

With advances in 3D content representation, diffusion models [11, 44] begin to play a predominant role in 3D generation [12, 25, 31]. Among different 3D representations, 3D Gaussians [15] have gained popularity for modeling 3D scenes and objects due to their high efficiency, explicit structure, and superior rendering quality. Notably, training diffusion models to generate 3D Gaussians requires high-quality “ground truth” 3D Gaussians, which must be pre-fitted to the 3D objects [10, 27, 46].

To advance the community, we constructed a large-scale dataset named **GaussianVerse**, comprising high-quality 3D

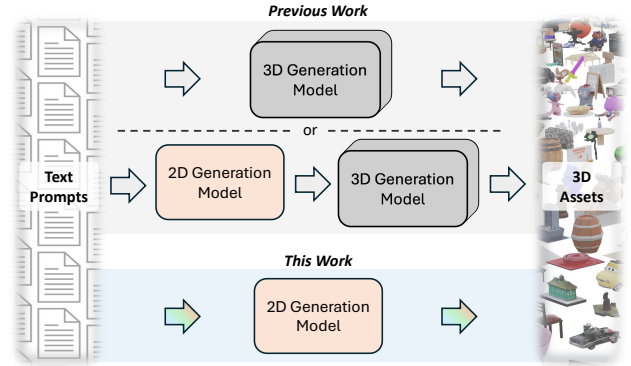


Figure 1. Previous 3D generators are either end-to-end 3D models [10, 57] or a combination of a multi-view 2D generator followed by a 2D-to-3D lifting model [49, 54]. In this work, we achieve 3D object generation by directly fine-tuning 2D generation models.

Gaussian fittings for a diverse range of objects. Unlike previous studies that also pre-compute 3D Gaussian references, *GaussianVerse* provides higher-quality fittings with the minimum required number of Gaussians, through a novel pruning strategy and a more effective, but compute-intensive, fitting process.

Designing standalone diffusion models for 3D generation is straightforward. However, such models have significant limitations especially when trained solely on 3D data, as high-quality 3D data is relatively scarce compared to 2D images. To achieve higher rendering fidelity in 3D generation, it is desirable to leverage the learned prior knowledge from well-pretrained 2D diffusion models [5, 21, 28, 33]. Some methods have been proposed to incorporate pre-trained 2D diffusion models with frozen weights into the 3D generation pipeline through complex designs, such as score-distilled sampling [33] and collaborative controls [5].

In this paper, we propose a fresh perspective that repurposes 2D diffusion models for 3D generation through direct fine-tuning. To fully harness the capabilities of these 2D diffusion models, we introduce **Gaussian Atlas**, a novel 2D representation of 3D Gaussians. This representation enables direct fine-tuning by first transporting unorganized 3D Gaussians into a standard 3D sphere and then apply-

\*Part of this work was done while Tiange Xiang was an intern at Meta Reality Labs, under the mentorship of Kai Li and Chengjiang Long.

†Corresponding authors.

ing equirectangular projection to map them into a square 2D grid, creating a Gaussian Atlas. We show that these Gaussian atlases facilitate transfer of the prior knowledge captured in 2D diffusion models to the 3D generation task. By doing so, our approach provides a means to leverage the learned 2D priors for 3D generation, unlocking new possibilities for efficient and effective 3D content creation.

To summarize, our major contributions are three-fold: (i) We present a large-scale dataset, **GaussianVerse**, consisting of 205,737 high-quality 3D Gaussian fittings for diverse objects sampled from Sketchfab [43]; (ii) We propose a novel 2D representation of 3D Gaussians, **Gaussian Atlas**, facilitating 3D generation tasks through a new perspective by fine-tuning pretrained 2D diffusion models; (iii) We demonstrate that the proposed approaches surpass state-of-the-art 3D Gaussian generators in terms of both generation-prompt alignment and user preferences.

## 2. Related Work

**Repurposing 2D diffusion models.** Diffusion models [6, 11, 37], are originally designed for text-to-image generation. When trained on large-scale internet images, prior knowledge learned from diverse domains can be transferred to different tasks. Marigold [14] is an example of how fine-tuning pretrained Latent Diffusion (LD) models [37] can benefit depth prediction. Marigold first re-parameterizes single-channel depth maps as RGB images and uses the pretrained VAE encoder to compress both the input image as well as its paired depth map into a shared latent space. The two latents are then concatenated to enable conditional generation of depth latents, which are subsequently decoded back into RGB space through the VAE decoder. More recent work, such as GeoWizard [7] and GenPercept [52], explored the repurposing of LD models for more geometric prediction tasks and beyond. As more and more studies have shown the potential of finetuning LD for different purposes, this work is among the first to explore how a LD model can be adapted for 3D generation, addressing the significant disparity between 3D objects and 2D images.

**3D generation with Gaussian splatting.** Unlike 2D images, 3D objects are more difficult to generate due to the additional dimension and geometric constraints [15, 29]. Among all 3D generation methods [4, 16, 18, 35, 48, 49, 53], there is a line of work that utilizes diffusion models to generate 3D Gaussians, which is closely related to this paper. GSD [30] introduced rendering guidance to constrain the sampling of 3D Gaussians with 2D observations. L3DG [36] is another example, which embeds 3D Gaussians onto a dense latent grid and learns a diffusion model in the latent space for generation. Moreover, GVGen [10] and GaussianCube [57] achieve 3D Gaussian diffusion by transforming sparsely located Gaussians into more structured 3D vol-

umes. GVGen fits 3D Gaussians directly on a volume with offsets, while GaussianCube applies Optimal Transport to move 3D Gaussians to vertices of a predefined 3D grid. Gaussian Anything [17] adopts a two-step approach that generates Gaussians by auto-encoding point cloud latents. Recently, TRELLIS [51] designed a structured representation that supports decoding to various 3D formats. In this work, we propose to transform 3D Gaussians onto 2D atlases, to leverage the power of well pretrained 2D diffusion models and unify the architecture of 2D and 3D generation.

**2D representations of 3D content.** Representing 3D objects as 2D planes is not new. A major line of research encodes 3D structures using implicit Triplanes [3]. NFD [42] was one of the first attempts to train 2D diffusion models to generate Triplanes, from which neural fields can be derived to reconstruct 3D objects. To enhance 3D coherence, CRM [49] integrates multi-view observations into the Triplane generation process. InstantMesh [53] and Instant3D [18] follow a similar design but employ more sophisticated models to improve Triplane synthesis. Instead of generating neural fields, TriplaneGaussian [60] decodes 3D Gaussian attributes directly from generated Triplanes. More recently, DiffGS [59] has refined the TriplaneGaussian paradigm by learning a mapping between pre-fitted 3D Gaussians and Triplanes via a latent diffusion model. Several works share motivations similar to ours. For example, PI3D [21] fine-tunes a pretrained text-to-image generation model to produce Triplanes represented as “pseudo-images”, while HexaGen3D [28] leverages pretrained image diffusion models for improved Triplane generation. However, their fine-tuned diffusion models exhibit limited capacity, and an additional minutes-long refinement process is typically required to enhance the 3D generation.

In addition to Triplane-based representations, Splatter Image [45] trains a 2D network to infer pixel-wise Gaussian attributes from single images; Omegas [55] trains 2D diffusion models to fit 2D UV maps of the geometry and materials of 3D objects, ultimately reconstructing a textured 3D mesh. However, Omegas supports only class-conditioned generations of a limited pre-defined categories; GIMDiffusion [5] adopts a similar approach by representing the surface of 3D objects with geometry images [8] and leveraging 2D diffusion models in the UV space; DiffSplat [19] trains VAE to compress multi-view 3D Gaussians into 2D latents and achieve multi-view generation through a pretrained 2D diffusion model. In contrast, our method introduces a more dense 2D representation of 3D Gaussians, yielding a novel approach for repurposing pretrained 2D diffusion models.

## 3. GaussianVerse

In this section, we present GaussianVerse, a large-scale dataset containing high-quality 3D Gaussian fittings for a





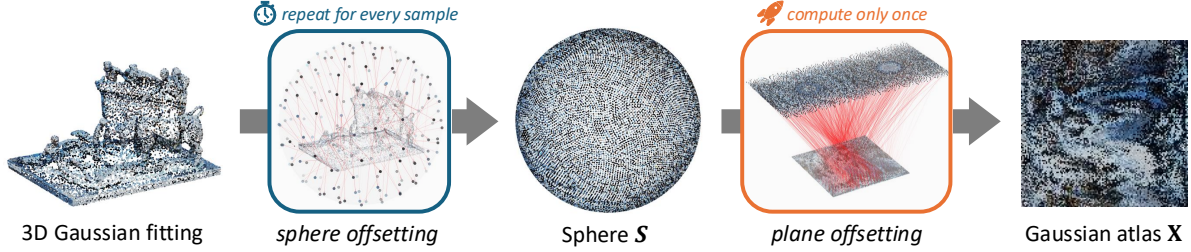


Figure 3. **Representing 3D Gaussians as 2D Gaussian Atlas.** For each fitting, 3D Gaussians are first translated to the surface of a standard sphere  $S$  via optimal transport. Then, the surface Gaussians are flattened onto the 2D plane via equirectangular projection with reusable indices. We obtain Gaussian Atlas by reorganizing the flattened coordinates to pixels of a dense 2D square of size  $\sqrt{N} \times \sqrt{N}$ .

negated structural similarity index,  $\mathcal{L}_{lips}$  is the perceptual loss, and  $\mathcal{R}$  is a scaling regularization term [24]. The  $\lambda$ 's are weights for each loss. Note that the addition of perceptual loss nearly doubles the training time, but it is necessary for high rendering fidelity with fewer Gaussians.

**Dataset details.** GaussianVerse consists of **205,737** 3DGS fittings of 3D objects sampled from Sketchfab [43] under CC licenses. We used the multi-view 2D renderings provided in [61] to perform per-object fittings. The 2D renderings came in 10 different categories, and we used renderings from 9 of the categories, excluding those of 'poor quality'. This curated list results in a wide coverage of diverse objects. We visualize a word cloud as well as the top 20 most frequent words from the captions [26] in Figure 2 (b) and (c). For optimal efficiency and quality balance [10, 57], we set the bound  $\tau$  to  $192 \times 192 = 36,864$ . A cluster of A100 GPUs is employed for large-scale parallel fitting. Each 3DGS fitting job converges at around 20,000 steps, translating to approximately 10 minutes of fitting time per object, with a total of **over 3.8 A100 GPU years** spent.

**Comparison with related work.** Compared with several previous studies [10, 30, 57] which also fit per-object 3D Gaussians for training diffusion models, we achieve higher-quality 3DGS fittings with fewer valid Gaussians but increased compute costs with a refined pruning strategy and a more effective, but compute-intensive, fitting process.

#### 4. Formulating 3D Gaussians as 2D Atlas

In this section, we introduce a novel approach that transforms unorganized Gaussians in the 3D space to a dense 2D representation, namely Gaussian Atlas, making it possible to repurpose 2D diffusion models, for example, Latent Diffusion (LD) [37], for 3D generation tasks.

**Motivation.** LD can understand complex natural language and generate coherent 2D images, benefiting from the vast availability of over billions of paired text-image data [40]. However, text-to-3D generation presents greater challenges due to two key reasons: (i) the scarcity of large-scale datasets with 3D models comparable to those in 2D, as creating and annotating high-quality, textured 3D models

remains both resource-intensive and time-consuming [26]; and (ii) the inherently higher-dimensional nature of 3D object representations, which impose complex geometric constraints, making it more difficult for diffusion models to interpret. These disparities in data availability and representational complexity between 2D and 3D motivate our approach to leveraging learned priors from pre-trained 2D diffusion models for 3D Gaussian generation.

However, unstructured Gaussians in 3D space cannot be directly passed to 2D models, which require inputs  $\mathbf{X}$  to have: (i) only 2 spatial dimensions; (ii) valid "pixels" at each vertex of a dense 2D grid; and (iii) values within a specific distribution, either  $\mathbf{X} \in [-1, 1]$  for the VAE or  $\mathbf{X} \sim \mathcal{N}(0, 1)$  for the denoiser. To make 3D Gaussians compatible with 2D diffusion models, we propose **Gaussian Atlas**, a 2D representation of 3D Gaussians.

One simple idea of 2D transformation is to project 3DGS onto an image plane with their 3D coordinates and given camera parameters. However, this naive approach loses depth information entirely and disrupts the original 3D structure's topology, which is essential for 3D generation as it relies on accurate representation of 3D continuity. This highlights the need for a method that not only maps 3D Gaussians onto a 2D plane but also preserves 3D continuity to some extent. Given these requirements, we argue that methods similar to UV texture unwrapping, which unfold the surface of a 3D geometry onto a 2D plane, are more suitable. However, UV maps are usually not universally applicable since careful designs are needed for different 3D geometries [1, 9]. Therefore, instead of exact mappings between 3D geometries and their 2D UVs, we focus on one characteristic of UV unwrapping — geometry flattening.

Specifically, our goal is to find a mapping function  $\mathcal{M}(\cdot)$  that transforms the 3D positions  $\{\mathbf{x} \in \mathbb{R}^3\}$  of 3D Gaussians to 2D planar coordinates  $\{\hat{\mathbf{x}} \in \mathbb{R}^2\}$ :  $\mathcal{M}(\{\mathbf{x}\}) \rightarrow \{\hat{\mathbf{x}}\}$ . A natural approach is to parameterize such a function  $\mathcal{M}$  as neural networks which can be optimized toward 2D and 3D consistency [58]. However, this approach requires repeated training of  $\mathcal{M}$  on different objects which is not only time consuming but also makes the mapping process inconsistent between objects given that the heuristics for 2D flatten-



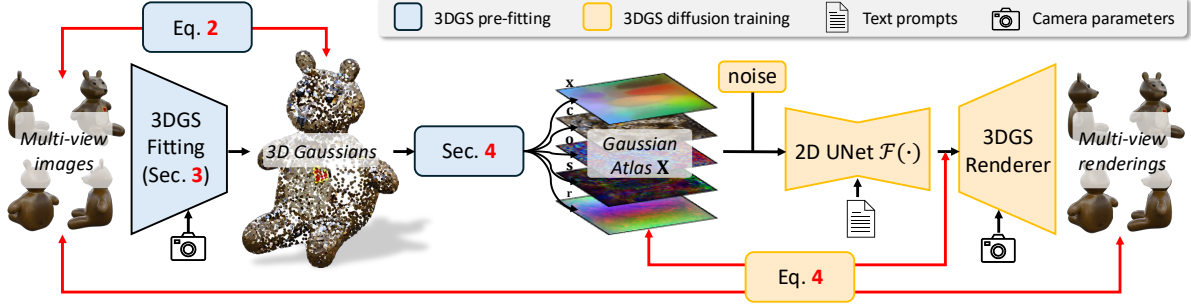


Figure 4. **Repurposing 2D diffusion models for 3D Gaussian generation.** Our pipeline consists of two stages. In the 3DGS pre-fitting stage (section 3), we pre-fit high quality 3D Gaussians for a diverse array of 3D objects with multi-view observations. The large-scale 3DGS fittings are then re-structured as Gaussian Atlas (section 4) with 2D representations for each 3DGS attribute. In the diffusion model training stage (section 5), we leverage the transformed 2D Gaussian atlases to repurpose a pretrained latent diffusion model (the 2D UNet denoiser  $\mathcal{F}$ ) and ultimately achieve 3D content generation.

ing may be different for different geometries. As a result, diffusion models are not able to capture the irregular patterns and fail to generate meaningful contents. Experiments are provided in section 6.2 to support this claim. To this end, we seek a more coherent transformation between 3D and 2D with a simple and deterministic mapping function.

We formulate our transformation process into three sequential stages, as outlined in Figure 3. In the first stage, we hypothesize a unit sphere  $\mathcal{S}$ , which is centered at the origin of 3D-axis with unit radius, to be parameterized by  $N$  3D points  $\{s_i \in \mathbb{R}^3\}$  that are uniformly distributed on its surface. Sphere is a well-studied structure that offers multiple standards for 2D projection, which makes it suitable for being considered in the flattening process. We then translate the unorganized 3D Gaussians to the surface points  $\{s_i \in \mathbb{R}^3\}$  of  $\mathcal{S}$  using Optimal Transport (OT) [2]. We call this process *sphere offsetting*. Our method differs from [57] by offsetting 3D Gaussians directly onto the *surface*, rather than vertices *within* a volume. Our transportation process is also much faster due to the adaptive number of Gaussians.

After positioning the 3D Gaussians on the surface of a unit sphere, we employ equirectangular projection [50] as our  $\mathcal{M}$  to obtain flattened 2D coordinates  $\{p_i \in \mathbb{R}^2\}$  of the 3D Gaussians. Lastly, in the *plane offsetting* stage, we apply another OT to map  $\{p_i\}$  to the vertices  $\{q_i \in \mathbb{R}^2\}$  of a square 2D grid with spatial size  $\sqrt{N} \times \sqrt{N}$ , further reducing sparsity. In particular, since now  $\mathcal{M}$  is a deterministic function, the mapping between  $\{p_i\}$  and  $\{q_i\}$  remains identical for all objects. This consistency allows us to perform OT in the last stage only once and reuse the computed indices for all objects. We refer to the final grid-like 2D representation of 3D Gaussians as Gaussian Atlas, with each atlas  $\mathbf{X}$  in the shape of  $\sqrt{N} \times \sqrt{N} \times (||\mathbf{x} - \mathbf{s}|| + ||\mathbf{c}|| + ||\mathbf{o}|| + ||\mathbf{s}|| + ||\mathbf{r}||)$  entailing all attributes of 3D Gaussians.

## 5. 2D Diffusion for 3D Gaussian Generation

After transforming fitted 3D Gaussians onto 2D planes, we are able to fine-tune the pre-trained Latent Diffusion (LD) [37] with Gaussian atlases.

**Preliminaries: Latent Diffusion.** LD is a family of models that generate 2D images based on text prompts. The core components of LD include a Variational AutoEncoder (VAE) and a UNet  $\mathcal{F}(\cdot)$ . The VAE encoder compresses images into lower-dimensional latents  $l$  to facilitate efficient diffusion in the latent space. By injecting Gaussian noise to the latents,  $\mathcal{F}$  can be trained through self-supervised denoising via v-parameterization [39]:

$$\mathcal{L}_{diff} = \mathbb{E}_{l_0, \mathbf{z}, t} \left[ \|\nabla_{l_t} \mathbf{z} - \nabla_{l_t} \mathcal{F}(l_t, t)\|^2 \right], \quad (3)$$

where  $l_t$  is the noisy latent at timestamp  $t$ ,  $\nabla_{l_t} \mathbf{z}$  is the ‘velocity’ added to  $l_t$ . During inference, a sample can be generated through the reverse diffusion process by iteratively forwarding  $\mathcal{F}$  for denoising. The VAE decoder then upsamples the generated latent back to the original RGB space.

**Finetuning LD with Gaussian Atlases.** The standard fine-tuning approach for LDs involves VAE-based encoding and decoding [14]. However, in the supplementary materials, we argue that such auto-encoding is unsuitable for Gaussian atlases - the Gaussian attributes differ from the natural images used to train the LD. Finetuning LD UNet with 2D atlases is feasible only if the distributions of the atlases are aligned with the VAE-encoded latents. We therefore standardize the 2D atlases using the pixel-wise mean and standard deviation computed from the entire GaussianVerse. This normalization prevents extreme high- or low-frequency pixel values while preserving the characteristics of the original VAE-encoded image latents, ultimately accelerating the fine-tuning process.

3D Gaussians are characterized by five attributes: the 3D location (mean)  $\mathbf{x}$ , albedo  $\mathbf{c}$ , and scale  $\mathbf{s}$ , each represented as three-channel features; opacity  $\mathbf{o}$ , which is a

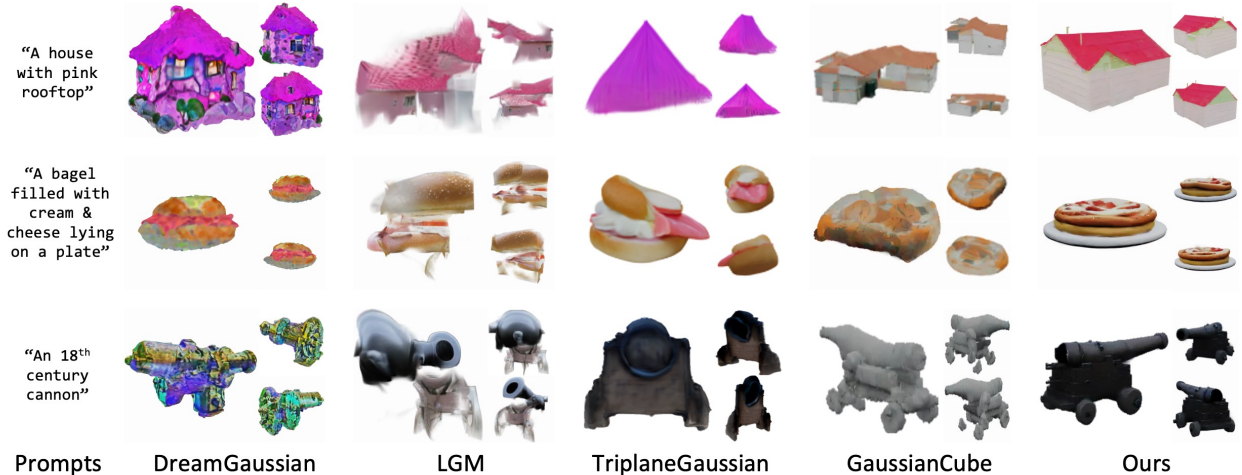


Figure 5. **Qualitative Comparisons.** Our 3D generations exhibit the highest quality, minimal artifacts, and the best alignment with text prompts. In contrast, DreamGaussian [46], LGM [47], and TriplaneGaussian [60] struggle to produce natural and complete 3D assets, while GaussianCube [57] fails to capture key phrases in text prompts, such as “on a plate” and “pink rooftop”.

single-channel feature; and rotation  $\mathbf{r}$ , typically represented as a four-channel quaternion. Since the LD UNet was originally trained on four-channel latents, we pad each three-channel attribute with the one-channel opacity and repeat the input layer of the UNet four times [7, 14] to accommodate all attributes as inputs. The final Gaussian atlases, used for fine-tuning the UNet, have a shape of  $128 \times 128 \times 16$ . During rendering, we appropriately unpack the different attributes and average the three repetitions of opacity.

We finetune the LD UNet  $\mathcal{F}$  with a combination of diffusion loss (Equation 3) and photometric loss between the renderings from denoised Gaussians and the reference images. The final objective for tuning  $\mathcal{F}$  becomes:

$$\lambda_{diff}\mathcal{L}_{diff} + \lambda_{rgb}\mathcal{L}_{rgb} + \lambda_{mask}\mathcal{L}_{mask} + \lambda_{lips}\mathcal{L}_{lips}, \quad (4)$$

where  $\mathcal{L}_{rgb}$ ,  $\mathcal{L}_{mask}$  are L1 loss on RGB renderings and accumulated opacity maps and  $\mathcal{L}_{lips}$  is the perceptual loss.  $\lambda$ s are the loss weights. Our pipeline is outlined in Figure 4.

## 6. Experiments

In this section, we benchmark and evaluate our proposed methods on zero-shot text-to-3D generation, one of the most fundamental tasks in generative 3D modeling.

**Implementation Details.** Given the upper bound  $\tau = 36,864$  of valid 3D Gaussians during the pre-fitting stage, we set the total number of 3D Gaussians per Gaussian atlas to  $N = 16,384 = 128 \times 128$ . This choice of  $N$  accommodates the large variance of 3D Gaussians in GaussianVerse.

We initialize the 2D UNet  $\mathcal{F}$  from a LD pretrain checkpoint [40] and use CLIP [34] to encode text prompts. The UNet is then fine-tuned with classifier-free guidance by randomly zeroing out the text encodings with a probability of

20%. We employ the AdamW optimizer [22] with a learning rate of  $5 \times 10^{-5}$  and a batch size of 64. Exponential Moving Average (EMA) and mixed precision training are enabled for stable and efficient training. For fair comparisons with the baseline method [57], only approximately 130K atlases from GaussianVerse were used for training. The paired text prompts were from [26] and the multi-view references were from [61]. The LD UNet was finetuned for 1M steps on 8 A100 GPUs.

For inference, we start from 2D random noise in the same shape as a Gaussian atlas and generate clean samples via reverse diffusion using the adaptive DPMsolver++ [23] with a guidance scale of 3.5. A 3DGS sample can be generated and rendered in less than 5 seconds.

**Metrics.** Reference based metrics are not feasible for evaluating zero-shot text-to-3D generations. Following [13, 33, 57], we evaluate the alignment of text prompts and 10 random 2D renderings of the 3D generations with CLIP score [34] as well as VQA score [20] on 100 diverse test prompts. Additional user studies and qualitative comparisons were also conducted for comprehensive evaluations.

**Comparisons.** We compare our proposed method against four representative methods in the field of 3D Gaussian generation: An optimization based method — DreamGaussian [46]; A method uses also a 2D model — LGM [47]; A method generates also 2D representations — TriplaneGaussian [60]; and the state-of-the-art 3D Gaussian generator with a 3D diffusion model — GaussianCube [57]. For LGM and TriplaneGaussian, we utilize MVDream [41] to generate 2D images from text prompts to initiate 3D generations. Notably, since there are no open-source implementations of the relevant works that also adopt 2D representations of 3D

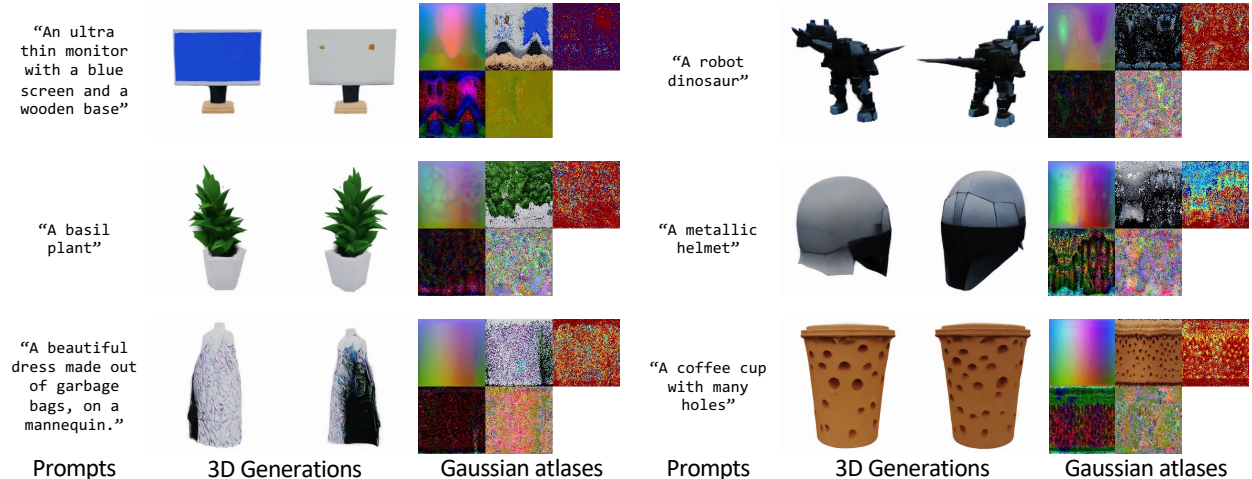


Figure 6. **Additional qualitative results.** Our method effectively repurposes 2D diffusion models for high-quality 3D contents. The generated Gaussian atlases are presented in the order from top left to bottom right: 3D location  $\mathbf{x}$ , albedo  $\mathbf{c}$ , color-coded opacity  $\mathbf{o}$ , normalized scale  $\mathbf{s}$ , and the last three channels of normalized quaternion  $\mathbf{r}$ . *More results can be found in the supplementary materials.*

Methods	CLIP score $\uparrow$	VQA score $\uparrow$	# Gaussians $\downarrow$
DreamGaussian [46]	20.52	0.37	40K
LGM [47]	20.28	0.35	66K
TriplaneGaussian [60]	21.10	0.46	<b>16K</b>
GaussianCube [57]	22.31	0.52	33K
GaussianAtlas (Ours)	<b>23.20</b>	<b>0.61</b>	<b>16K</b>

Table 2. **Qualitative comparisons.** Our method achieves performance comparable to the state-of-the-art in terms of CLIP similarity scores, with the minimum number of 3D Gaussians.

content [5, 21, 28], direct comparisons are not possible.

## 6.1. Results

**Qualitative results.** We present text-to-3D generation results in Figure 5. Compared to DreamGaussian and LGM, our generations exhibit high visual fidelity without excessive details. In contrast to TriplaneGaussian and GaussianCube, our method aligns closely with the text prompts, reflecting more precise prompt conditioning. According to the additional results shown in Figure 6, our fine-tuned 2D diffusion model is capable of generating high-quality Gaussian atlases. Consequently, our generated 3D contents are coherent and self-contained, with no seams or artifacts that would typically be observed from UV unwrapping methods.

**Quantitative results.** In Table 2, we present the CLIP and VQA scores for comparison methods. Our method outperforms all counterparts while generating the minimum number of Gaussians required. Specifically, it uses only  $\frac{1}{2}$  the number of Gaussians and the number of training steps on 3D data compared to GaussianCube, achieving a CLIP score higher by 0.9 and a VQA score higher by 17%. This further supports our claim that pretrained 2D diffusion models can be repurposed for 3D content generation.

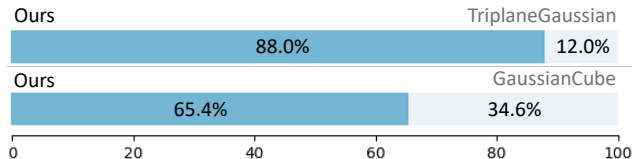


Figure 7. **User study results.** Our method outperforms state-of-the-art methods [57, 60] in user preferences regarding generation quality and alignment with text prompts.

**User studies<sup>1</sup>.** The user study was conducted with diverse participants who were asked to assess the overall generation quality to given text prompts. They performed pairwise comparisons between generations by our method and those from a competing method. We calculated the win rate from  $> 2,500$  valid responses. As shown in Figure 7, over 65% of users preferred the 3D content generated by our method when compared to GaussianCube. The preference rate was even more pronounced against TriplaneGaussian, with 88% of users favoring our method.

## 6.2. Discussions and Ablations

This work takes a step toward unifying 2D and 3D generation by transforming 3D Gaussians onto 2D planes, allowing the direct fine-tuning of a pre-trained 2D diffusion model for generating 3D contents. In this section, we conduct extensive studies and ablative experiments to validate our proposed approach from three key perspectives.

- *Learned knowledge in text-to-image diffusion models is universally transferable.* Without pre-training on large-scale 2D data, the model struggles to develop a comprehensive understanding of natural language and content generation when trained solely on 3D data. As shown in Figure 8,

<sup>1</sup>The user study was conducted entirely by researchers at Stanford.



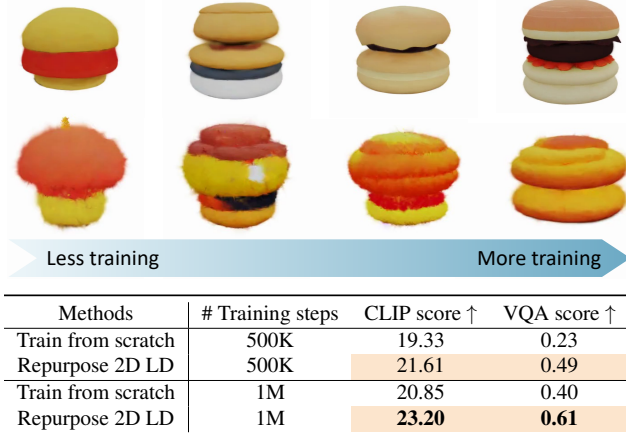


Figure 8. Finetuning from a pretrained 2D diffusion model leads to *faster* generalization. **Top:** 3D generations at different training checkpoints from finetuning (top row) and training from scratch (bottom row) using the same prompt ‘A toy hamburger with beef patty & cheese’. **Bottom:** Quantitative comparisons at checkpoints with different training steps.

we effectively repurpose the pre-trained 2D diffusion model with faster convergence and higher-quality 3D generation. The qualitative results show that, compared to training from scratch, our approach produces more coherent and structured 3D assets earlier in training. The quantitative results further support this finding, as our repurposed models consistently achieve higher scores in different training steps.

- *Gaussian atlases yield consistent and capturable visual patterns, which makes the pre-trained 2D diffusion model easier to generalize towards.* To validate the claim, we ablate on the “flattening” strategy and adopted an optimization based approach [58] to find the most natural cut for each object and perform 3D-to-2D transformation via a combination of neural networks. We train the networks on a per-object basis for the entire GaussianVerse, which roughly took another A100 GPU year. The flattened 3D Gaussians are then used to finetune the LD UNet by following the same training procedure. We visualize generation results in Figure 9. With capturable visual patterns, our proposed flattening strategy leads to faster model convergence and much higher generation quality at the same training step.

- *A pre-trained 2D diffusion model serves as a better initialization for 3D generation.* In Figure 10, we plot the weight differences between our fine-tuned UNet and both a randomly initialized UNet and the pre-trained UNet directly from LD. We observe overall small changes in the weights from the pre-trained UNet. Even at the layer with the greatest change, the difference is still  $8\times$  smaller than that from a random initialization. This indicates that the pre-trained LD weights provide better starting points for 3D generation, facilitating easier convergence to a local minimum.

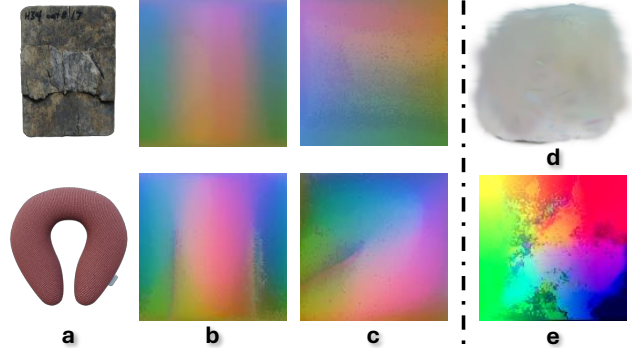


Figure 9. The optimization-based flattening approach results in inconsistent patterns that are hard for fine-tuning. We show two objects (a) and their Gaussian atlases (3D location  $x$  only) obtained using our proposed flattening approach (b) and the optimization-based approach [58] (c), which generates only noisy Gaussians (d) and atlases (e) after training for the same number of steps.

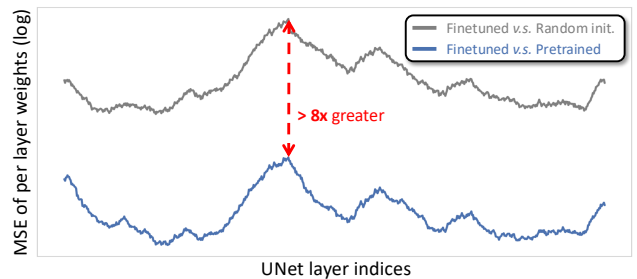


Figure 10. Log scale mean squared errors (smoothed) of per layer weights between different UNets. Finetuning from a pre-trained LD UNet leads to smaller weight differences.

## 7. Conclusion

This paper presents an advancement in unifying 2D and 3D content generation by repurposing a pre-trained 2D diffusion models to generate 3D Gaussians. Historically, finetuning 2D diffusion models with 3D Gaussians was infeasible. We introduce Gaussian Atlas, a novel approach that transforms unorganized 3D Gaussians into a structured 2D grid, thereby enabling the effective utilization of 2D networks for 3D generation. We also present GaussianVerse, a large-scale dataset comprising 205,737 3D Gaussian fittings of diverse 3D objects, which facilitates diffusion model training. Experiments demonstrate that our method achieves state-of-the-art 3D generation results using significantly fewer Gaussians. We also provide extensive discussions and ablation studies that validate our claims and offer valuable insights into the effectiveness of our approach.

**Acknowledgments.** Tiange Xiang, Scott Delp, Ehsan Adeli, and Li Fei-Fei’s work at Stanford were partially funded by the NIH Grant R01AG089169 and P41EB027060, Panasonic Holdings Corporation, the Gordon and Betty Moore Foundation, the Jaswa Innovator Award, Stanford HAI, Stanford HAI graduate

fellowship, and Stanford Wu Tsai Human Performance Alliance. We thank Fei Jiang and Moustafa Meshry for their insightful feedback on this work.

## References

- [1] Haoran Bai, Di Kang, Haoxian Zhang, Jinshan Pan, and Linchao Bao. Ffhq-uv: Normalized facial uv-texture dataset for 3d face reconstruction. In *Proceedings of the IEEE/CVF conference on computer vision and pattern recognition*, pages 362–371, 2023. 4
- [2] Rainer E Burkard and Eranda Cela. Linear assignment problems and extensions. In *Handbook of combinatorial optimization: Supplement volume A*, pages 75–149. Springer, 1999. 5
- [3] Eric R Chan, Connor Z Lin, Matthew A Chan, Koki Nagano, Boxiao Pan, Shalini De Mello, Orazio Gallo, Leonidas J Guibas, Jonathan Tremblay, Sameh Khamis, et al. Efficient geometry-aware 3d generative adversarial networks. In *Proceedings of the IEEE/CVF conference on computer vision and pattern recognition*, pages 16123–16133, 2022. 2
- [4] Zhaoxi Chen, Jiaxiang Tang, Yuhao Dong, Ziang Cao, Fangzhou Hong, Yushi Lan, Tengfei Wang, Haozhe Xie, Tong Wu, Shunsuke Saito, et al. 3dtopia-xl: Scaling high-quality 3d asset generation via primitive diffusion. *arXiv preprint arXiv:2409.12957*, 2024. 2
- [5] Slava Elizarov, Ciara Rowles, and Simon Donné. Geometry image diffusion: Fast and data-efficient text-to-3d with image-based surface representation. *arXiv preprint arXiv:2409.03718*, 2024. 1, 2, 7
- [6] Patrick Esser, Sumith Kulal, Andreas Blattmann, Rahim Entezari, Jonas Müller, Harry Saini, Yam Levi, Dominik Lorenz, Axel Sauer, Frederic Boesel, et al. Scaling rectified flow transformers for high-resolution image synthesis. In *Forty-first International Conference on Machine Learning*, 2024. 2
- [7] Xiao Fu, Wei Yin, Mu Hu, Kaixuan Wang, Yuexin Ma, Ping Tan, Shaojie Shen, Dahua Lin, and Xiaoxiao Long. Geowizard: Unleashing the diffusion priors for 3d geometry estimation from a single image. In *European Conference on Computer Vision*, pages 241–258. Springer, 2024. 2, 6
- [8] Xianfeng Gu, Steven J Gortler, and Hugues Hoppe. Geometry images. In *Proceedings of the 29th annual conference on Computer graphics and interactive techniques*, pages 355–361, 2002. 2
- [9] Rıza Alp Güler, Natalia Neverova, and Iasonas Kokkinos. Densepose: Dense human pose estimation in the wild. In *Proceedings of the IEEE conference on computer vision and pattern recognition*, pages 7297–7306, 2018. 4
- [10] Xianglong He, Junyi Chen, Sida Peng, Di Huang, Yangguang Li, Xiaoshui Huang, Chun Yuan, Wanli Ouyang, and Tong He. Gvgen: Text-to-3d generation with volumetric representation. *arXiv preprint arXiv:2403.12957*, 2024. 1, 2, 4
- [11] Jonathan Ho, Ajay Jain, and Pieter Abbeel. Denoising diffusion probabilistic models. *Advances in neural information processing systems*, 33:6840–6851, 2020. 1, 2
- [12] Yicong Hong, Kai Zhang, Jiuxiang Gu, Sai Bi, Yang Zhou, Difan Liu, Feng Liu, Kalyan Sunkavalli, Trung Bui, and Hao Tan. Lrm: Large reconstruction model for single image to 3d. *arXiv preprint arXiv:2311.04400*, 2023. 1
- [13] Ajay Jain, Ben Mildenhall, Jonathan T Barron, Pieter Abbeel, and Ben Poole. Zero-shot text-guided object generation with dream fields. In *Proceedings of the IEEE/CVF conference on computer vision and pattern recognition*, pages 867–876, 2022. 1, 6
- [14] Bingxin Ke, Anton Obukhov, Shengyu Huang, Nando Metzger, Rodrigo Caye Daudt, and Konrad Schindler. Repurposing diffusion-based image generators for monocular depth estimation. In *Proceedings of the IEEE/CVF Conference on Computer Vision and Pattern Recognition*, pages 9492–9502, 2024. 2, 5, 6, 1
- [15] Bernhard Kerbl, Georgios Kopanas, Thomas Leimkühler, and George Drettakis. 3d gaussian splatting for real-time radiance field rendering. *ACM Trans. Graph.*, 42(4):139–1, 2023. 1, 2, 3
- [16] Yushi Lan, Fangzhou Hong, Shuai Yang, Shangchen Zhou, Xuyi Meng, Bo Dai, Xingang Pan, and Chen Change Loy. Ln3diff: Scalable latent neural fields diffusion for speedy 3d generation. In *European Conference on Computer Vision*, pages 112–130. Springer, 2024. 2
- [17] Yushi Lan, Shangchen Zhou, Zhaoyang Lyu, Fangzhou Hong, Shuai Yang, Bo Dai, Xingang Pan, and Chen Change Loy. Gaussiananything: Interactive point cloud latent diffusion for 3d generation. *arXiv preprint arXiv:2411.08033*, 2024. 2
- [18] Jiahao Li, Hao Tan, Kai Zhang, Zexiang Xu, Fujun Luan, Yinghao Xu, Yicong Hong, Kalyan Sunkavalli, Greg Shakhnarovich, and Sai Bi. Instant3d: Fast text-to-3d with sparse-view generation and large reconstruction model. *arXiv preprint arXiv:2311.06214*, 2023. 2
- [19] Chenguo Lin, Panwang Pan, Bangbang Yang, Zeming Li, and Yadong Mu. Diffplat: Repurposing image diffusion models for scalable gaussian splat generation. *arXiv preprint arXiv:2501.16764*, 2025. 2
- [20] Zhiqiu Lin, Deepak Pathak, Baiqi Li, Jiayao Li, Xide Xia, Graham Neubig, Pengchuan Zhang, and Deva Ramanan. Evaluating text-to-visual generation with image-to-text generation. In *European Conference on Computer Vision*, pages 366–384. Springer, 2024. 6
- [21] Ying-Tian Liu, Yuan-Chen Guo, Guan Luo, Heyi Sun, Wei Yin, and Song-Hai Zhang. Pi3d: Efficient text-to-3d generation with pseudo-image diffusion. In *Proceedings of the IEEE/CVF Conference on Computer Vision and Pattern Recognition*, pages 19915–19924, 2024. 1, 2, 7
- [22] I Loshchilov. Decoupled weight decay regularization. *arXiv preprint arXiv:1711.05101*, 2017. 6
- [23] Cheng Lu, Yuhao Zhou, Fan Bao, Jianfei Chen, Chongxuan Li, and Jun Zhu. Dpm-solver++: Fast solver for guided sampling of diffusion probabilistic models. *arXiv preprint arXiv:2211.01095*, 2022. 6
- [24] Tao Lu, Mulin Yu, Linning Xu, Yuanbo Xiangli, Limin Wang, Dahua Lin, and Bo Dai. Scaffold-gs: Structured 3d gaussians for view-adaptive rendering. In *Proceedings of*

- the *IEEE/CVF Conference on Computer Vision and Pattern Recognition*, pages 20654–20664, 2024. 3, 4, 1
- [25] Shitong Luo and Wei Hu. Diffusion probabilistic models for 3d point cloud generation. In *Proceedings of the IEEE/CVF conference on computer vision and pattern recognition*, pages 2837–2845, 2021. 1
- [26] Tiange Luo, Chris Rockwell, Honglak Lee, and Justin Johnson. Scalable 3d captioning with pretrained models. *arXiv preprint arXiv:2306.07279*, 2023. 3, 4, 6
- [27] Qi Ma, Yue Li, Bin Ren, Nicu Sebe, Ender Konukoglu, Theo Gevers, Luc Van Gool, and Danda Pani Paudel. Shap-splat: A large-scale dataset of gaussian splats and their self-supervised pretraining, 2024. 1, 2
- [28] Antoine Mercier, Ramin Nakhli, Mahesh Reddy, Rajeev Yasarla, Hong Cai, Fatih Porikli, and Guillaume Berger. Hexagen3d: Stablediffusion is just one step away from fast and diverse text-to-3d generation. *arXiv preprint arXiv:2401.07727*, 2024. 1, 2, 7
- [29] Ben Mildenhall, Pratul P Srinivasan, Matthew Tancik, Jonathan T Barron, Ravi Ramamoorthi, and Ren Ng. Nerf: Representing scenes as neural radiance fields for view synthesis. *Communications of the ACM*, 65(1):99–106, 2021. 2
- [30] Yuxuan Mu, Xinxin Zuo, Chuan Guo, Yilin Wang, Juwei Lu, Xiaofeng Wu, Songcen Xu, Peng Dai, Youliang Yan, and Li Cheng. Gsd: View-guided gaussian splatting diffusion for 3d reconstruction. *arXiv preprint arXiv:2407.04237*, 2024. 2, 3, 4
- [31] Alex Nichol, Heewoo Jun, Prafulla Dhariwal, Pamela Mishkin, and Mark Chen. Point-e: A system for generating 3d point clouds from complex prompts. *arXiv preprint arXiv:2212.08751*, 2022. 1
- [32] William Peebles and Saining Xie. Scalable diffusion models with transformers. In *Proceedings of the IEEE/CVF International Conference on Computer Vision*, pages 4195–4205, 2023. 3
- [33] Ben Poole, Ajay Jain, Jonathan T Barron, and Ben Mildenhall. Dreamfusion: Text-to-3d using 2d diffusion. *arXiv preprint arXiv:2209.14988*, 2022. 1, 6
- [34] Alec Radford, Jong Wook Kim, Chris Hallacy, Aditya Ramesh, Gabriel Goh, Sandhini Agarwal, Girish Sastry, Amanda Askell, Pamela Mishkin, Jack Clark, et al. Learning transferable visual models from natural language supervision. In *International conference on machine learning*, pages 8748–8763. PMLR, 2021. 6
- [35] Xuanchi Ren, Jiahui Huang, Xiaohui Zeng, Ken Museth, Sanja Fidler, and Francis Williams. Xcube: Large-scale 3d generative modeling using sparse voxel hierarchies. In *Proceedings of the IEEE/CVF Conference on Computer Vision and Pattern Recognition*, pages 4209–4219, 2024. 2
- [36] Barbara Roessle, Norman Müller, Lorenzo Porzi, Samuel Rota Bulò, Peter Kontschieder, Angela Dai, and Matthias Nießner. L3dg: Latent 3d gaussian diffusion. *arXiv preprint arXiv:2410.13530*, 2024. 2, 3
- [37] Robin Rombach, Andreas Blattmann, Dominik Lorenz, Patrick Esser, and Björn Ommer. High-resolution image synthesis with latent diffusion models. In *Proceedings of the IEEE/CVF Conference on Computer Vision and Pattern Recognition*, pages 10684–10695, 2022. 2, 4, 5
- [38] Nataniel Ruiz, Yuanzhen Li, Varun Jampani, Yael Pritch, Michael Rubinstein, and Kfir Aberman. Dreambooth: Fine tuning text-to-image diffusion models for subject-driven generation. In *Proceedings of the IEEE/CVF conference on computer vision and pattern recognition*, pages 22500–22510, 2023. 3
- [39] Tim Salimans and Jonathan Ho. Progressive distillation for fast sampling of diffusion models. *arXiv preprint arXiv:2202.00512*, 2022. 5
- [40] Christoph Schuhmann, Romain Beaumont, Richard Vencu, Cade Gordon, Ross Wightman, Mehdi Cherti, Theo Coombes, Aarush Katta, Clayton Mullis, Mitchell Wortsman, et al. Laion-5b: An open large-scale dataset for training next generation image-text models. *Advances in Neural Information Processing Systems*, 35:25278–25294, 2022. 4, 6
- [41] Yichun Shi, Peng Wang, Jianglong Ye, Mai Long, Kejie Li, and Xiao Yang. Mvdream: Multi-view diffusion for 3d generation. *arXiv preprint arXiv:2308.16512*, 2023. 6, 2
- [42] J Ryan Shue, Eric Ryan Chan, Ryan Po, Zachary Ankner, Jiajun Wu, and Gordon Wetzstein. 3d neural field generation using triplane diffusion. In *Proceedings of the IEEE/CVF Conference on Computer Vision and Pattern Recognition*, pages 20875–20886, 2023. 2
- [43] Sketchfab. Sketchfab: Publish & find 3d models online. <https://sketchfab.com/>, 2023. Accessed: 2023-10-05. 2, 4
- [44] Yang Song, Jascha Sohl-Dickstein, Diederik P Kingma, Abhishek Kumar, Stefano Ermon, and Ben Poole. Score-based generative modeling through stochastic differential equations. *arXiv preprint arXiv:2011.13456*, 2020. 1
- [45] Stanislaw Szymanowicz, Chrisitian Rupprecht, and Andrea Vedaldi. Splatter image: Ultra-fast single-view 3d reconstruction. In *Proceedings of the IEEE/CVF conference on computer vision and pattern recognition*, pages 10208–10217, 2024. 2
- [46] Jiayang Tang, Jiawei Ren, Hang Zhou, Ziwei Liu, and Gang Zeng. Dreamgaussian: Generative gaussian splatting for efficient 3d content creation. *arXiv preprint arXiv:2309.16653*, 2023. 1, 6, 7
- [47] Jiayang Tang, Zhaoxi Chen, Xiaokang Chen, Tengfei Wang, Gang Zeng, and Ziwei Liu. Lgm: Large multi-view gaussian model for high-resolution 3d content creation. In *European Conference on Computer Vision*, pages 1–18. Springer, 2024. 6, 7
- [48] Dmitry Tochilkin, David Pankratz, Zexiang Liu, Zixuan Huang, Adam Letts, Yangguang Li, Ding Liang, Christian Laforte, Varun Jampani, and Yan-Pei Cao. Tripso: Fast 3d object reconstruction from a single image. *arXiv preprint arXiv:2403.02151*, 2024. 2
- [49] Zhengyi Wang, Yikai Wang, Yifei Chen, Chendong Xi, Shuo Chen, Dajiang Yu, Chongxuan Li, Hang Su, and Jun Zhu. Crm: Single image to 3d textured mesh with convolutional reconstruction model. *arXiv preprint arXiv:2403.05034*, 2024. 1, 2



- [50] Wikipedia contributors. Equirectangular projection — Wikipedia, the free encyclopedia, 2024. [Online; accessed 7-November-2024]. [5](#)
- [51] Jianfeng Xiang, Zelong Lv, Sicheng Xu, Yu Deng, Ruicheng Wang, Bowen Zhang, Dong Chen, Xin Tong, and Jiaolong Yang. Structured 3d latents for scalable and versatile 3d generation. In *Proceedings of the Computer Vision and Pattern Recognition Conference*, pages 21469–21480, 2025. [2](#)
- [52] Guangkai Xu, Yongtao Ge, Mingyu Liu, Chengxiang Fan, Kangyang Xie, Zhiyue Zhao, Hao Chen, and Chunhua Shen. What matters when repurposing diffusion models for general dense perception tasks? *arXiv preprint arXiv:2403.06090*, 2024. [2](#)
- [53] Jiale Xu, Weihao Cheng, Yiming Gao, Xintao Wang, Shenghua Gao, and Ying Shan. Instantmesh: Efficient 3d mesh generation from a single image with sparse-view large reconstruction models. *arXiv preprint arXiv:2404.07191*, 2024. [2](#)
- [54] Yinghao Xu, Zifan Shi, Wang Yifan, Hansheng Chen, Ceyuan Yang, Sida Peng, Yujun Shen, and Gordon Wetzstein. Grm: Large gaussian reconstruction model for efficient 3d reconstruction and generation. *arXiv preprint arXiv:2403.14621*, 2024. [1](#)
- [55] Xingguang Yan, Han-Hung Lee, Ziyu Wan, and Angel X Chang. An object is worth 64x64 pixels: Generating 3d object via image diffusion. *arXiv preprint arXiv:2408.03178*, 2024. [2](#)
- [56] Hu Ye, Jun Zhang, Sibor Liu, Xiao Han, and Wei Yang. Ip-adapt: Text compatible image prompt adapter for text-to-image diffusion models. *arXiv preprint arXiv:2308.06721*, 2023. [3](#)
- [57] Bowen Zhang, Yiji Cheng, Jiaolong Yang, Chunyu Wang, Feng Zhao, Yansong Tang, Dong Chen, and Baining Guo. Gaussiancube: Structuring gaussian splatting using optimal transport for 3d generative modeling. *arXiv preprint arXiv:2403.19655*, 2024. [1](#), [2](#), [3](#), [4](#), [5](#), [6](#), [7](#)
- [58] Qijian Zhang, Junhui Hou, Wenping Wang, and Ying He. Flatten anything: Unsupervised neural surface parameterization. *arXiv preprint arXiv:2405.14633*, 2024. [4](#), [8](#)
- [59] Junsheng Zhou, Weiqi Zhang, and Yu-Shen Liu. Diffgs: Functional gaussian splatting diffusion. *Advances in Neural Information Processing Systems*, 37:37535–37560, 2024. [2](#)
- [60] Zi-Xin Zou, Zhipeng Yu, Yuan-Chen Guo, Yangguang Li, Ding Liang, Yan-Pei Cao, and Song-Hai Zhang. Triplane meets gaussian splatting: Fast and generalizable single-view 3d reconstruction with transformers. In *Proceedings of the IEEE/CVF Conference on Computer Vision and Pattern Recognition*, pages 10324–10335, 2024. [2](#), [6](#), [7](#)
- [61] Qi Zuo, Xiaodong Gu, Yuan Dong, Zhengyi Zhao, Weihao Yuan, Lingteng Qiu, Liefeng Bo, and Zilong Dong. High-fidelity 3d textured shapes generation by sparse encoding and adversarial decoding. In *European Conference on Computer Vision*, 2024. [4](#), [6](#)

# Repurposing 2D Diffusion Models with Gaussian Atlas for 3D Generation

## Supplementary Material

### A. Supplementary for GaussianVerse

#### A.1. Fitting Details

As described in Section 3, we adopted Scaffold-GS [24] as the base model for per-object 3D Gaussian fitting. We observed duplicated Gaussians when the number of offsets was large, even at the default value. Therefore, we reduced the number to 4 to allow more anchors to be initialized with random values. The 3D Gaussians were then optimized according to the objective in Equation 2, with  $\lambda'_{rgb}$  set to 0.8,  $\lambda'_{ssim}$  set to 0.2,  $\lambda'_{lips}$  set to 0.02, and  $\lambda'_{reg}$  set to 0.01.

#### A.2. 3DGS Quality of GaussianVerse

We compare our proposed 3DGS fitting method in Section 3 with the densification-constrained fitting method introduced by GaussianCube [57] and the upper-bound method, Scaffold-GS [24], in Figure 11. Compared to GaussianCube, our method achieves better rendering quality. Compared to the upper bound, our results show no significant visual degradation while using significantly fewer 3D Gaussians. As shown in Figure 11, the rendering quality of fitted 3DGS does not improve with an increased number of Gaussians. This observation confirms that many Gaussians contribute minimally to the final rendering quality and can be merged or pruned during fitting.

#### A.3. Comparison with Other 3D Gaussian Datasets

GaussianVerse is a large-scale dataset consisting of high-quality 3D Gaussian fittings for a wide range of objects. We note that there are a few other studies that also fit per-object 3D Gaussians to assist in the training of diffusion models. A direct comparison is provided in Table 3.

### B. Supplementary for Gaussian Atlas Formulation

#### B.1. Formulation Details

As discussed in Section 4, the adaptive nature of 3DGS fittings in GaussianVerse enables faster transformation of 3DGS to 2D Gaussian Atlas compared to the similar process in [57]. Notably, the computation time is significantly reduced during the non-square Optimal Transport step for *sphere offsetting*, since the number of 3D positions  $\{\mathbf{x}\}$  is typically much smaller than  $N$ , the number of surface points  $\{s\}$  on the standard sphere  $S$ . After sphere offsetting, for 3DGS fittings that have a smaller size than  $N$ , we pad additional Gaussians by duplicating the ones with the smallest scales and set their opacity to 0. For 3DGS fittings that have more Gaussians than  $N$ , we prune the Gaussians with the



Figure 11. **Comparisons of 3DGS fitting methods.** Our method achieves high fitting quality comparable to the upper bound with significantly fewer valid 3D Gaussians with positive opacity.

smallest scales before sphere offsetting. In practice, constructing one Gaussian atlas takes an average of approximately one minute.

### C. Supplementary for Finetuning LD with Gaussian Atlas

#### C.1. Training Diffusion Model Without VAEs

The typical fine-tuning approach involves VAE encoding and decoding [14]. However, we argue that such a VAE auto-encoding is inappropriate for Gaussian atlases due to three reasons: (i) VAE encoding is a lossy compression of the atlases, whose accuracy is crucial for Gaussian rendering. We demonstrate the impact of using VAE for auto-encoding Gaussian atlases in Figure 12; (ii) Even at the maximum bound  $\tau = 36,864 = 192 \times 192$ , the number of Gaussians is significantly smaller than the number of pixels required for VAE input (e.g.,  $768 \times 768$ ). Naive up-sampling of the Gaussian Atlas  $\mathbf{X}$  would significantly increase computational costs; (iii) Even with scaling and shifting,  $\mathbf{X}$  does not visually resemble the natural RGB images originally used for VAE training, but rather analogizes latent features. Considering these, we remove the original VAE and fine-tune the LD UNet directly on Gaussian atlases. We make appropriate modifications to the input and output layers of the UNet to accommodate all Gaussian attributes with the correct number of channels [14].

#### C.2. More Details

**Diffusion model training.** We set  $\lambda_{diff}$  to 1.0,  $\lambda_{rgb}$  to 10.0,  $\lambda_{mask}$  to 1.0, and  $\lambda_{lips}$  to 1.0 to finetune the LD

Methods	Venue	# of 3DGS fittings	# of Gaussians per fitting
GSD [30]	ECCV 2024	6,000	1,024
GVGen [10]	ECCV 2024	~46,000	32,768
GaussianCube [57]	NeurIPS 2024	125,653	32,768
ShapeSplat [27]	3DV 2025	~65,000	>20,000
<b>GaussianVerse (ours)</b>	-	205,737	10,435

Table 3. GaussianVerse contains large-scale 3DGS fittings with adaptive number of Gaussians, which allows various applications.

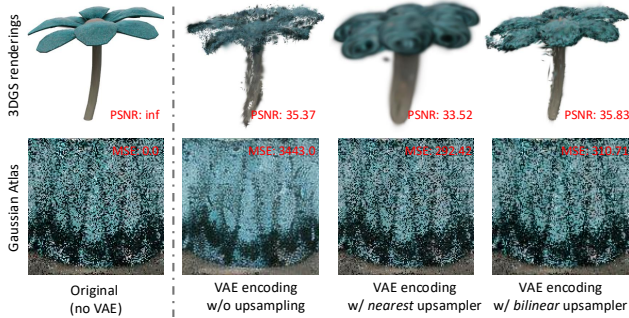


Figure 12. **Latent diffusion VAE degrades 3D Gaussian quality.** In the bottom row, we present a transformed Gaussian atlas and its reconstruction with and without VAE auto-encoding. When the atlas is up-sampled to a higher resolution, no obvious differences are observed in the atlas. However, after rendering the decoded Gaussians to images, we can observe much higher disparities, resulting in significantly reduced PSNR and visual quality. This suggests that incorporating the VAE for 3DGS diffusion is impractical.

UNet. At each training step, we randomly sample one view of 2D renderings to compute the photometric losses. We enable gradient checkpoint to save GPU memory, which allows a local batch size of 8 for each GPU, with a total batch size of 64 across 8 GPUs.

## D. More Results

### D.1. More Comparisons

Since Omages [55] does not support text-to-3D generation and the implementations of PI3D [21], HexaGen3D [28], and GIMDiffusion [5] are not publicly available, we provide additional qualitative comparisons against Splatter Image [45], a method that also generates 2D representations of 3D objects. As shown in Figure 13, while Splatter Image reconstructs the complete geometry of 3D objects with few artifacts, it struggles to generate coherent appearances with meaningful details. In contrast, our method leverages the prior knowledge embedded in a pre-trained 2D diffusion model, thereby yielding significantly improved generation quality.



Figure 13. **Comparison with a 2D generation approach [45].** Note that we provide MVDream [41] generated 2D images (shown as the main images) to initialize 3D generations of [45] (shown as the smaller images).

### D.2. More Generations

More results generated from a diverse list of prompts are shown in Figure 16 and Figure 17. We demonstrate impressive generation quality on text prompts involving descriptions for color, shape, style, abstract semantics, and quantities for objects. Additionally, we include videos of 360-degree renderings of the generated objects along with the supplementary material.

2D flattening and surface cutting may introduce unexpected artifacts in the final 3D generations [5]. However, when rendering the generated 2D atlases back as 3D Gaussians, no defects are observed at the 'seams' of disconnected 2D boundaries, and our final 3D generations are coherent and natural, similar to other direct 3D generation approaches [10, 57]. This proves the concept of our approach — 3D generation achieved by a 2D diffusion model.

### D.3. Diversity of Generations

With the same text prompt, we initiate the reverse diffusion with different random noise to demonstrate the diversity of generations in Figure 14. We observe a high diversity of geometries and appearances of the generated objects. This further proves that our proposed 2D representations of 3D Gaussians does not negatively alter the underlying semantics of the original 3D properties.



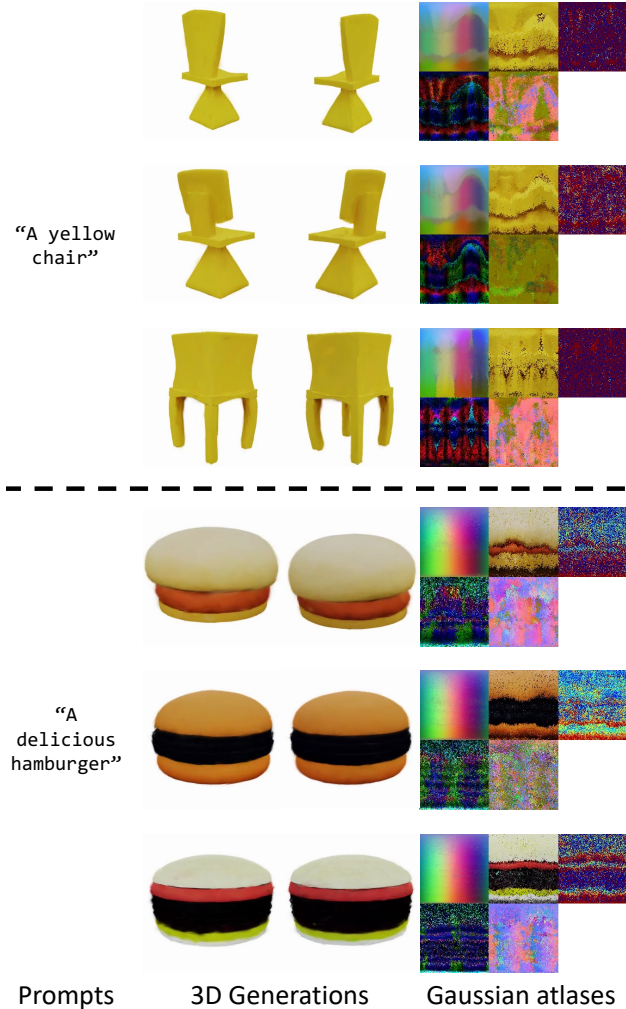


Figure 14. **Diverse text-to-3D generation results from the same prompt.** We present the generated Gaussian atlases in the order from top left to bottom right: 3D location  $\mathbf{x}$ , albedo  $\mathbf{c}$ , color-coded opacity  $\mathbf{o}$ , normalized scale  $\mathbf{s}$ , and the last three channels of normalized quaternion  $\mathbf{r}$ .

## E. Discussions

**Limitations.** Our experiments revealed a trade-off between generation quality and the parameter  $N$ , which denotes the number of Gaussians per Gaussian atlas. A larger  $N$  allows for finer-grained details in the generated outputs, but it also increases both training and inference costs. In this paper, we set  $N = 128 \times 128 = 16,384$  Gaussians as a good compromise between computational efficiency and quality. However, in our current setup — using approximately three times fewer Gaussians than in [57] — our 3D generations do not exhibit significantly finer details compared to state-of-the-art methods that employ substantially more Gaussians.

Moreover, since this work repurposes a specific checkpoint of the LD model, no major updates have been made

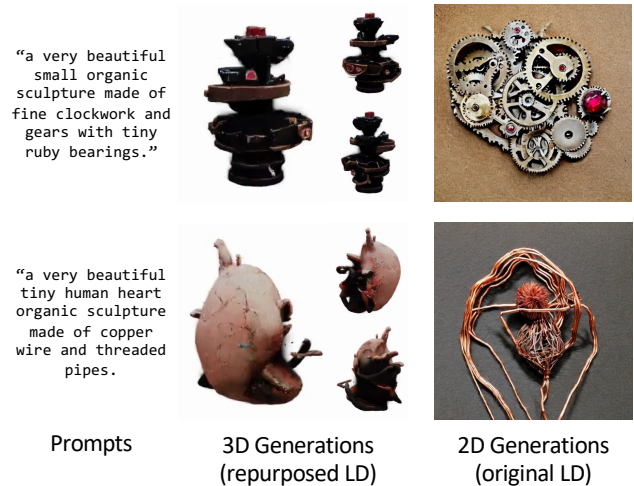


Figure 15. Similar to the original LD, our repurposed LD is not good at capturing long text prompts for 3D generations.

to the model architecture. Consequently, our model inherits the limitations of the original LD model for 3D generation, including reduced quality for long text prompts (see Figure 15).

**Future Directions.** The purpose of this work is to introduce a novel way to represent 3D contents as 2D and make attempts to unify both 2D and 3D generation, allowing advancements in either paradigm to benefit both. There are two directions particularly worth pursuing by following the pathway presented in this work. The first is to experiment with more advanced diffusion models, such as transformer-based architectures [32] or latent diffusion models for Gaussians [36]. The second is to integrate plug-ins that are originally designed for 2D diffusion models, such as IP-adapter [56] and DreamBooth [38], into 3D generations, given the unified diffusion framework.



Figure 16. **More text-to-3D generation results.** Our model is able to generate 2D Gaussian atlases to resemble high-quality 3D Gaussians from various prompts. We present the generated Gaussian atlases in the order from top left to bottom right: 3D location  $\mathbf{x}$ , albedo  $\mathbf{c}$ , color-coded opacity  $\mathbf{o}$ , normalized scale  $\mathbf{s}$ , and the last three channels of normalized quaternion  $\mathbf{r}$ .

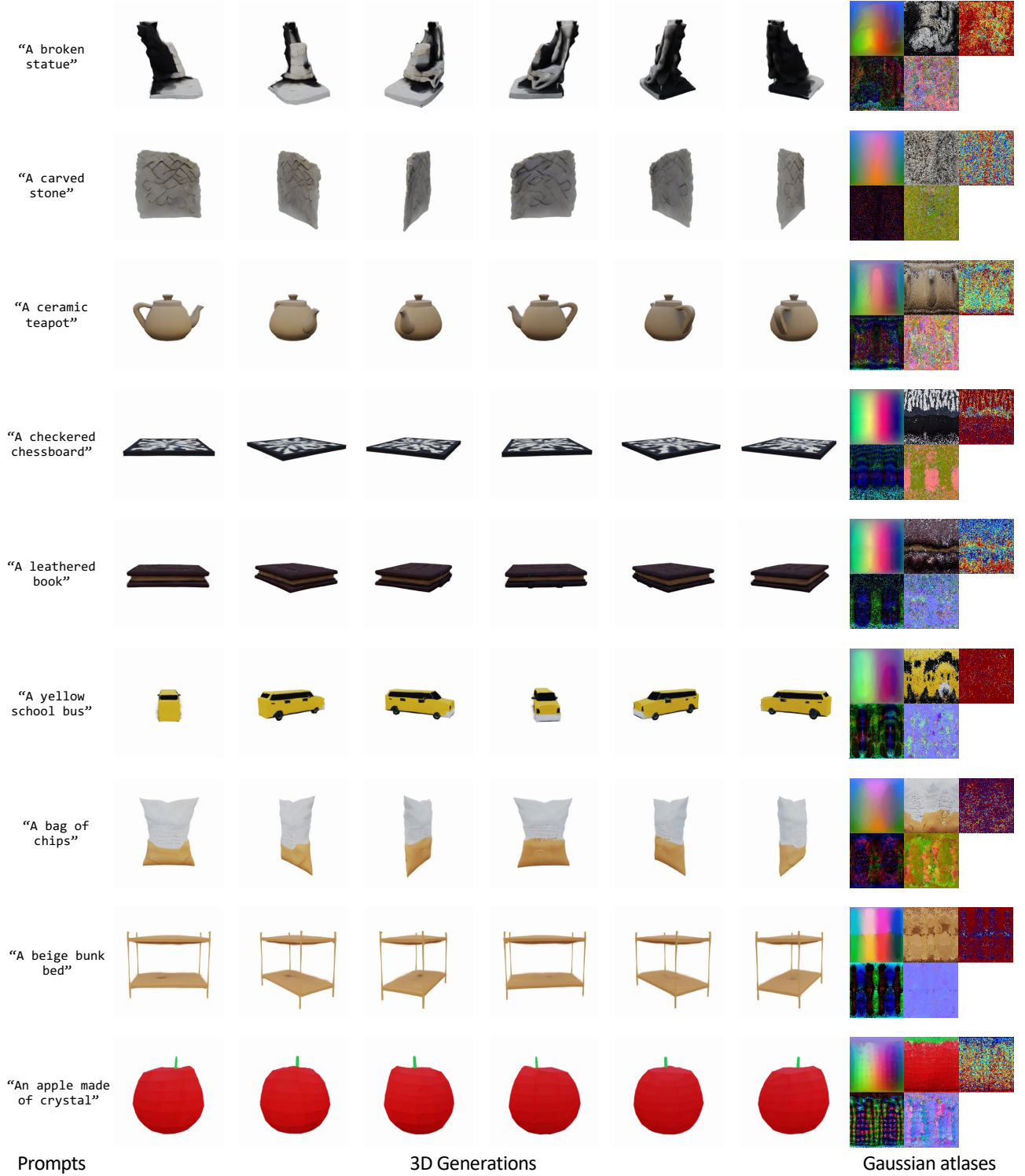


Figure 17. **More text-to-3D generation results (cont.).** Our model is able to generate 2D Gaussian atlases to resemble high-quality 3D Gaussians from various prompts. We present the generated Gaussian atlases in the order from top left to bottom right: 3D location  $x$ , albedo  $c$ , color-coded opacity  $o$ , normalized scale  $s$ , and the last three channels of normalized quaternion  $r$ .